Research Paper

Can molecular profiling enhance radiotherapy? Impact of personalized targeted gold nanoparticles on radiosensitivity and imaging of adenoid cystic carcinoma

Inbal Hazkani[1,2], Menachem Motiei[3], Oshra Betzer[3], Tamar Sadan[3], Dimitri Bragilovski[2], Leon Lubimov[2], Aviram Mizrachi[1,2], Tuvia Hadar[1,2], Mattan Levi[4], Irit Ben-Aharon[5], Izhack Haviv[6], Rachela Popovtzer[3✉] and Aron Popovtzer[1,2]

1. Sackler Faculty of Medicine, Tel-Aviv University, Ramat Aviv, Israel
2. Head and Neck Cancer Radiation Clinic, Institute of Oncology, Davidoff Cancer Center, Rabin Medical Center, Petach Tikva, Israel.
3. Faculty of Engineering & The Institute of Nanotechnology and Advanced Materials, Bar-Ilan University, Ramat Gan, Israel.
4. Department of Cell and Developmental Biology, Sackler Faculty of Medicine, Tel Aviv University, Tel Aviv, Israel
5. Institute of Oncology, Davidoff Cancer Center, Beilinson Hospital, Rabin Medical Center, Petach Tikva, Israel
6. Faculty of Medicine in the Galilee, Bar Ilan University, Ramat Gan, Israel.

✉ Corresponding author: Rachela Popovtzer, email: rachela.popovtzer@biu.ac.il

Abstract

Personalized molecular profiling has an established role in selection of treatment for metastatic disease; however, its role in improving radiosensitivity and functional imaging has not been evaluated. In the current study, we examined molecular profiling as a tool for designing personalized targeted gold nanoparticles (GNP) to serve as dual-modal tumor radiosensitizers and functional imaging enhancers. To this end, molecular profiling of a patient's salivary gland adenoid cystic carcinoma (ACC) was performed, and anaplastic lymphoma kinase (ALK) mutation was detected. The extracted tumor was subcutaneously injected into mice, which were then treated either with radiation, the specific ALK inhibitor crizotinib, or a combination of therapies. One of these combinations, namely, ALK-targeted GNP (via crizotinib coating), was found to enhance radiation treatment, as demonstrated by a significant decrease in tumor volume over 24 days. In parallel, ALK-targeted GNP substantially augmented tumor visualization via computed tomography. The mechanism of radiosensitivity enhancement was mostly related to a diminished cell repair mechanism in tumors, as demonstrated by proliferating cell nuclear antigen staining. These findings indicate that personalized molecular profiling is an effective technique for enhancing cancer theranostics.

Key words: Adenoid Cystic Carcinoma, Gold nanoparticles, crizotinib, molecular profiling, radiosensitizing agents, personalized imaging

Introduction

Adenoid cystic carcinoma (ACC) is a rare tumor, arising mostly in salivary and lacrimal glands. The tumor has characteristic clinical features of infrequent regional lymph node metastasis, and a prolonged, but relentlessly progressive clinical course, with high tendency for distant metastasis despite meticulous surgical treatment[1–3]. Late recurrence rates, both regionally and at distant sites, as well as death rates, are high[1,2]. Clinical outcome correlates with histologic grade, which, in turn, correlates with the degree of aneuploidy and genetic alterations present in the tumor genome [2].

Preoperative diagnostic imaging of ACC is performed with computed tomography (CT) and magnetic resonance imaging (MRI). Positron emission tomography CT (PET/CT) is used for initial staging

and evaluation of distant metastasis, yet tumors may not show enhanced fluorodeoxyglucose ([18]FDG) uptake or may be obscured by normal physiologic enhancement of salivary glands[4,5], leading to late detection of ACC in many cases.

The treatment of choice for primary salivary gland ACC (SACC) is surgery and post-operative radiation[3,6–8]. However, the efficacy of radiation has not been established[6–9]. The benefits of adjuvant radiation are unclear in terms of local control and survival, suggesting the involvement of radio-resistance in ACC[9]. Furthermore, use of chemo-radiation for treatment of local unresectable tumors and post-operative positive margin tumors remains controversial. In addition, due to the rarity of the disease and its heterogeneity, there is no consensus regarding the optimal treatment for metastatic or recurrent ACC[1–3,6].

Personalized treatment based on molecular profiling uses genomic characteristics of a patient's tumor to discover potential targets for treatment, as demonstrated in metastatic ACC[4,10-14] and a variety of other refractory cancers[10]. Profuse molecular alterations have been described in ACC as diagnostic, therapeutic and prognostic markers[4,11,12], and growing evidence shows an important role for molecular profiling in the decision process of pharmacological treatment for metastatic ACC[2–4,11,13–16]. Molecular profiling for ACC has been tested in several pilot studies, phase II trials and retrospective reviews, with some success[4,11–16]. However, there is no clear evidence for the contribution of this approach to radiation therapy treatment. Moreover, the use of radiosensitizing agents is only minimally endorsed in cancer, due to lack of clear biomarkers that can direct the use of this tool in patients who are likely to benefit from it.

Several studies have demonstrated the radiosensitizing effect of gold nanoparticles (GNP) when introduced into tumors. Particles composed of high atomic number materials, such as gold (Z=79), increase radiation sensitivity due to the significant increment in the absorption of photons and deposition of energy at the vicinity of the particles. Active targeting of GNP specifically to cancer biomarkers leads to high concentrations of gold selectively within tumors, thereby enhancing the radiation effect on the tumor, while sparing the surrounding normal tissue[17–26]. However, the mechanism underlying cell death caused by the radiosensitizing effect of GNP remains unclear; the main theories suggest increased apoptosis, intracellular reactive oxygen species or direct DNA damage[18,27].

In the current study, we performed molecular profiling of a major salivary gland ACC, in search for a potential biomarker for targeted radiosensitizing GNP. The profiling revealed an anaplastic lymphoma kinase (ALK) mutation, which has been shown to induce a constitutively activated tyrosine kinase receptor with pro-oncogenic effects[28–30]. Approximately 2% of all non-small cell lung cancers (NSCLC) are ALK positive[30].The presence of an ALK mutation in ACC is uncommon, and to date, no data has been published on the use of crizotinib, an ALK tyrosine kinase inhibitor[31], as treatment for ACC. Thus, our goals in the present study were three-fold. First, we examined whether coating of GNP with crizotinib can direct the particles to the tumor and thus lead to an enhanced radiosensitizing effect for treatment of ACC (Figure 1). Second, we evaluated the impact of targeted GNP on enhancement of tumor visualization using CT. Third, we investigated the biological mechanisms underlying tumor diminution following treatment with targeted GNP radiosensitizers.
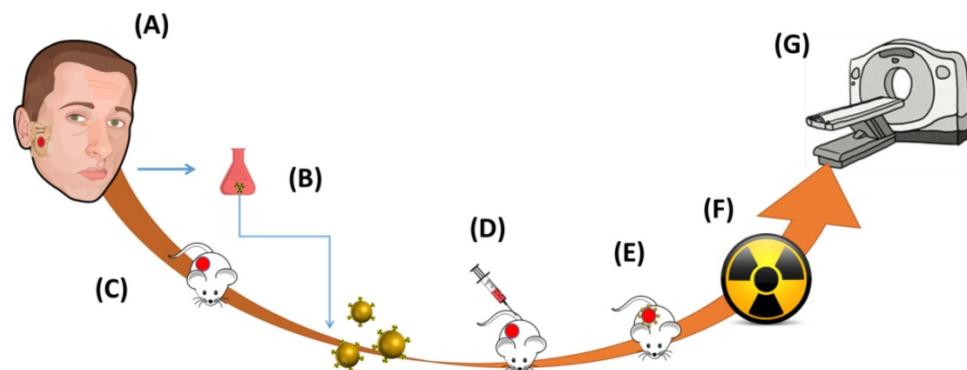

Figure 1. Assessing the impact of targeted GNP on radioenhancement. A. A sample was taken from the tumor of a patient with adenoid cystic carcinoma (ACC) of the parotid gland. B. Molecular profiling was performed on the tumor, identifying a target mutation, anaplastic lymphoma kinase. Gold nanoparticles (GNP) were prepared and coated with crizotinib, a tyrosine kinase inhibitor. C. 50 µl human ACC were subcutaneously injected into the back flank area of a nude mouse. D. Actively targeted GNP were injected to the tail vein of the mouse and E. accumulated at the tumor. F. Twelve hours post injection the mouse was irradiated once, and the tumor size was closely evaluated in vivo using micro CT and measurements.

Study Design

Molecular profiling of a patient's salivary gland Adenoid Cystic Carcinoma (ACC) was performed, and an anaplastic lymphoma kinase (ALK) mutation was detected. ACC tumors were then subcutaneously injected into mice. Mice were treated 40-50 days after ACC implementation, when the tumor size reached a diameter of 10 mm. To ensure a standardized tumor size at the time of treatment, size was defined by the calculated volume using the largest tumor diameters. Mice were treated with radiation (single fraction of 18 Gy) or anti-ALK (crizotinib) alone, or a combination of treatments with or without targeted GNP (as detailed in Table 1). All experiments were performed under general anesthesia. In groups 2, 4 and 6, radiation was administered **12** hours after injection of GNP.

Table 1. Summary of treatments in mice with an ACC xenograft.

Groups*	Type of treatment
Group 1	Control (no treatment)
Group 2	Radiation alone
Group 3	Crizotinib alone
Group 4	Radiation + crizotinib
Group 5	Crizotinib-GNP
Group 6	Radiation + crizotinib-GNP

*Each group included three mice, except for Groups 1 and 6 which included two mice each

Results

GNP characterization

On transmission electron microscopy (TEM), the GNP appeared as uniformly distributed spheres of 20 nm diameter (Figure 2A). An expanded signal on ultraviolet-visible spectroscopy and zeta potential results confirmed the chemical coating after each layer was completed (Figure 2B, C). Maintenance of the same plasmon resonance for 3 months confirmed the continued stability of the crizotinib monoclonal antibody-conjugated GNP.

Tumor volume

Mice received a subcutaneous injection of human ACC (50 µl) into the back flank, and treatments were given 40-50 days later (T0; when tumor diameter was 10 mm). Tumor volumes were examined in all groups over a period of 24 days after treatment (Figure 3).

Treatment with radiation alone or crizotinib+radiation was found to impede tumor growth as compared to untreated controls after 24 days (t-test, $p<0.001$), although both treatments did not significantly reduce tumor volume below its size at T0 (t-test, $p>0.05$). In contrast, treatment with radiation+crizotinib-GNP not only decreased tumor volume as compared to untreated controls ($p<0.001$), but also caused significant shrinkage of the tumor, to near disappearance, as compared to its size before treatment (t-test, $p=0.007$).

Closer examination of the groups treated with radiation revealed that targeted GNP and radiation had the most prominent effect on tumor volume. Crizotinib-GNP-radiation significantly reduced tumor volume as compared to crizotinib-radiation (without GNP) (t-test $p<0.01$) and radiation only ($p<0.05$), 24 days after treatment. The addition of crizotinib without GNP to the radiation therapy did not cause any difference in the tumor growth pattern as compared to radiation alone ($p=0.966$).

Treatment with crizotinib, either alone or conjugated to GNP, significantly decreased tumor volume after 24 days, as compared to untreated controls (t-test; $p<0.001$ for both), despite the fact that these groups were not irradiated. However, crizotinib-GNP showed significant reduction in tumor volume as compared to crizotinib alone (t-test, $p<0.001$). These results indicate a potential benefit from crizotinib as a treatment option. A possible explanation for the superior results of the crizotinib-GNP treated group is an increased accumulation of crizotinib in the tumor when conjugated to GNP, most probably due to the enhanced permeability and retention (EPR) effect[32].
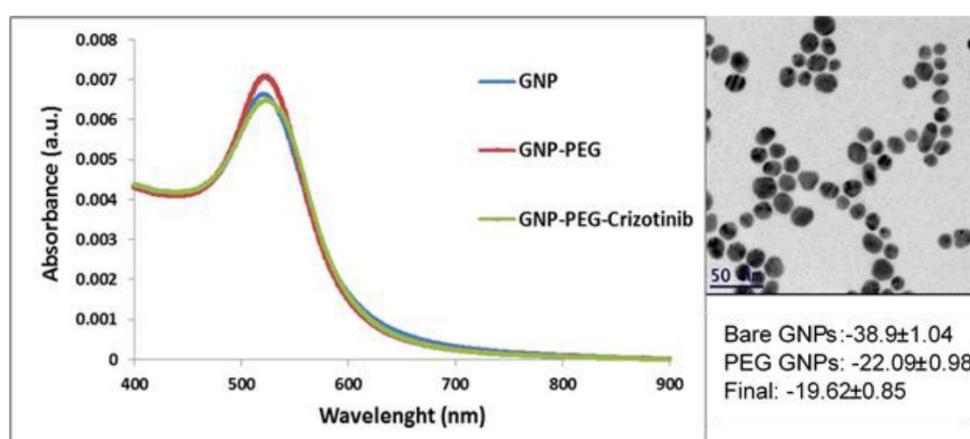

Bare GNPs: -38.9±1.04
PEG GNPs: -22.09±0.98
Final: -19.62±0.85

Figure 2: Characterizations of GNP. A: TEM image of 20nm GNP. B: Zeta Potential measurements. C: UV-vis spectroscopy of the bare GNP, PEGylated GNP, crizotinib-GNP.

Targeted GNP enhances ACC diagnosis using CT imaging

We additionally examined migration and accumulation of the targeted GNP at the tumor area, over time, using 3D whole-body volume rendering CT imaging.

A comparison of tumor imaging on day two after treatment shows that while the tumor is difficult to detect in the control group (Figure 4A), targeted GNP (Figure 4B) can be easily identified in the tumor area, thus providing a clear and definite diagnosis.

Figure 5 demonstrates the accumulation of directly targeted GNP (with crizotinib) in the radiation-treated tumor at 36 hours, six days and 24 days after injection. As seen in the figure, the accumulation of targeted GNP in the tumor is proportional to tumor size, and can be detected even when tumor volume is only a few cubic millimeters.

Gold Concentration in the Tumor

Flame atomic absorption spectroscopy (FAAS) analysis of the amount of GNP in the tumor, 24 days post radiation, demonstrated that the quantity of gold in the non-irradiated group was twice as high as in the irradiated group (0.675 GNP/gr-tissue, 11.23% of total GNP injected, and 0.318 GNP/gr-tissue,5.3% of total GNP injected, respectively).

FAAS analysis also showed that insignificant amounts of gold remained in the blood (average of 0.008 GNP/gr-tissue), kidney (average of 0.046 GNP/gr-tissue) and liver (average of 0.088 GNP/gr-tissue) in the irradiated and non-irradiated groups.

Biological mechanism of radiosensitizer-GNP

The histological effect of the various treatment arms was assessed using biopsy samples containing tumor and adjacent tissue, taken from treated mice 24 days post treatment. Immunohistochemistry was performed to examine tumor proliferation (Ki-67), DNA repair (proliferating cell nuclear antigen; PCNA) and vascularization (hematopoietic progenitor cell antigen; CD34), whereas terminal transferase-mediated deoxyuridine 5-triphosphate nick-end labeling (TUNEL) assay was used for apoptosis assessment. Tumor cells pre- and post-radiation showed equal ALK positive staining. In addition, ALK staining was more conspicuous in the crizotinib treatment groups, with or without radiation. However, the addition of GNP to crizotinib and radiation resulted in a weaker ALK staining. Ki-67 levels were weak in the radiation-only and crizotinib-only treatment groups as compared to the untreated control, and even weaker in the crizotinib-GNP-radiation group, indicating a prominent reduction in cell proliferation. A TUNEL assay showed no difference between the radiation-only group and the addition of crizotinib or crizotinib-GNP to radiation. PCNA staining was strongest in the crizotinib-GNP-radiation group, though marked staining was seen in the radiation-only group as compared to control. CD34 was considerably lower in the groups treated with radiation, with or without crizotinib or GNP (Figure 6).

Toxicity

Four of 16 mice died before the end of the study. All but one were treated with crizotinib only, and one mouse, which died after 24 days was treated with crizotinib-GNP-radiation. The remaining mice did not show any decline in well-being, as evaluated by food intake, weight, and behavioral parameters (neurological or coordination alterations).
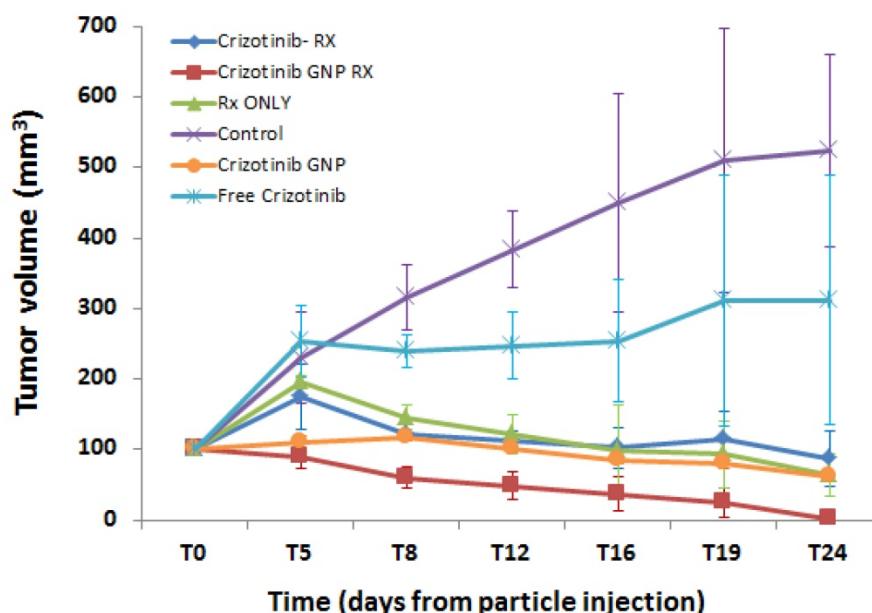

Figure 3: Average changes in tumor growth over 24 days after treatment. Shown are mice treated at T0 with either radiation only, crizotinib+radiation, or the combination of crizotinib-coated GNP and radiation. Tumor volume was monitored up to 24 days later (T24). Control mice remained untreated throughout this period. The combination of targeted GNP and radiation showed a gradual reduction in tumor volume, until near disappearance 24 days after treatment. Results presented as mean ± SEM (Standard Error of Mean) .Rx: radiation.

Discussion

ACC is a rare tumor with a high local recurrence rate and a tendency for distant metastasis despite meticulous surgical treatment[1–4]. The role and efficacy of radiation, though considered as standard therapy, has not been established[6–9]. In addition, molecular profiling can be used to identify potential targets for which there are available therapies, as was shown in other studies. Personalized treatment for ACC based on molecular profiling has been tested in several phase II trials and retrospective reviews, with some success[11,13–15]. In the present study, we examined molecular profiling as a tool for detecting factors that can target GNP to ACC, and thus improve imaging and radio sensitivity of these tumors. Using molecular profiling, we found ALK as a potential biomarker for ACC, and conjugated the ALK inhibitor crizotinib to GNP.

Tumor volume and radiosensitivity

Our results show that crizotinib-GNP injection was associated with a significant improvement in tumor radio sensitivity, manifested by a reduction in tumor volume, as compared to the other modalities examined. Both imaging (CT) and quantitative (FAAS) findings demonstrated accumulation of the targeted GNP in the tumor, which further asserts the role of targeted GNP in enhancement of radiation.

The aggregation of GNP-crizotinib in the tumor, and the favorable effect of GNP-crizotinib on tumor volume, are most probably due to the EPR effect, in which the permeability of tumor vasculature causes an accumulation of macromolecules such as targeted GNP in the tumor bed, which is not seen in normal tissue[32]. In addition, the finding that a smaller amount of GNP was present in the tumors of the irradiated group versus the non-irradiated group suggests that GNP are effective radio enhancers, as even half the amount of GNP sufficed to exert a significant radiation effect. We hypothesize that the smaller amount of GNP in the irradiated group is probably due to the decrease in tumor vasculature and blood flow caused by high-dose radiation[33],which limits the accumulation of GNP in the tumor. This hypothesis is supported by the weak CD 34 staining found in the irradiated groups.
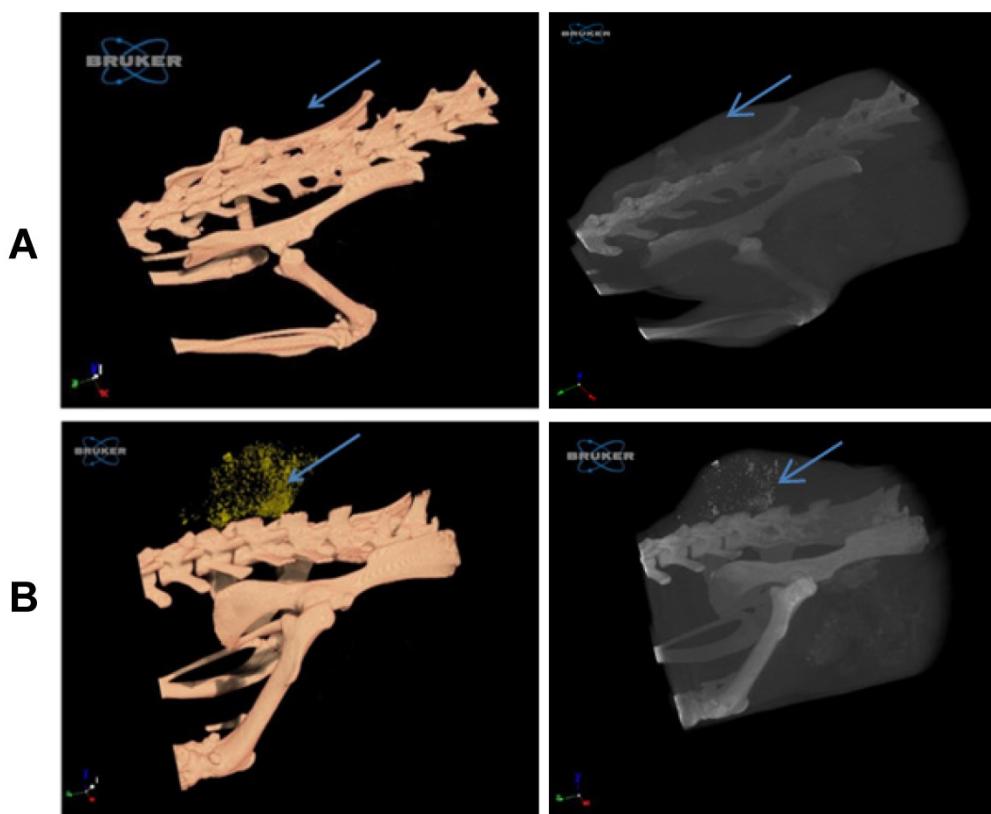

Figure 4. Imaging of the tumor with 3D whole-body volume rendering CT on day two. Scans of mice were performed with nominal resolution (pixel size) of 36 m, employing an aluminum filter 0.2 mm thick and an applied X-ray tube voltage of 45 kV. Surface-rendered 3D models were constructed for 3D viewing of the analyzed mice. (A) In the control group, the tumor is barely detected (left panel), while in the targeted GNP group (B) the tumor is easily observed by the gold accumulation (yellow dots; left panel). The GNP can also be seen as white dots in the tumor (right panel, black and white 3D volume CT image). Arrow indicates the tumor in all panels.
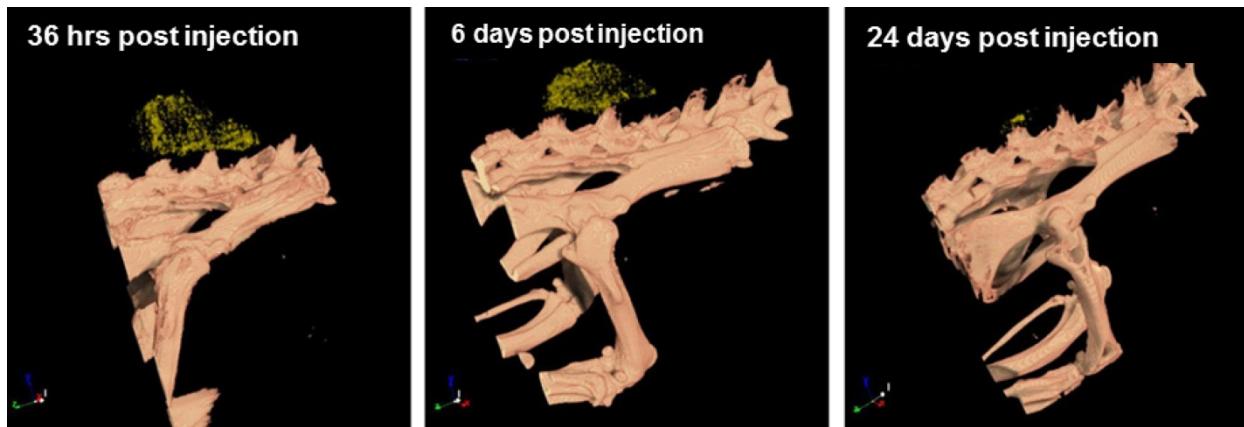
Figure 5. Post radiation targeted GNP accumulation in the tumor, over time. 3D volume-rendering images show accumulation of GNP (yellow dots) can be seen 36 hours, six days and 24 days post injection, clearly showing the gradual shrinkage of the tumor over time.
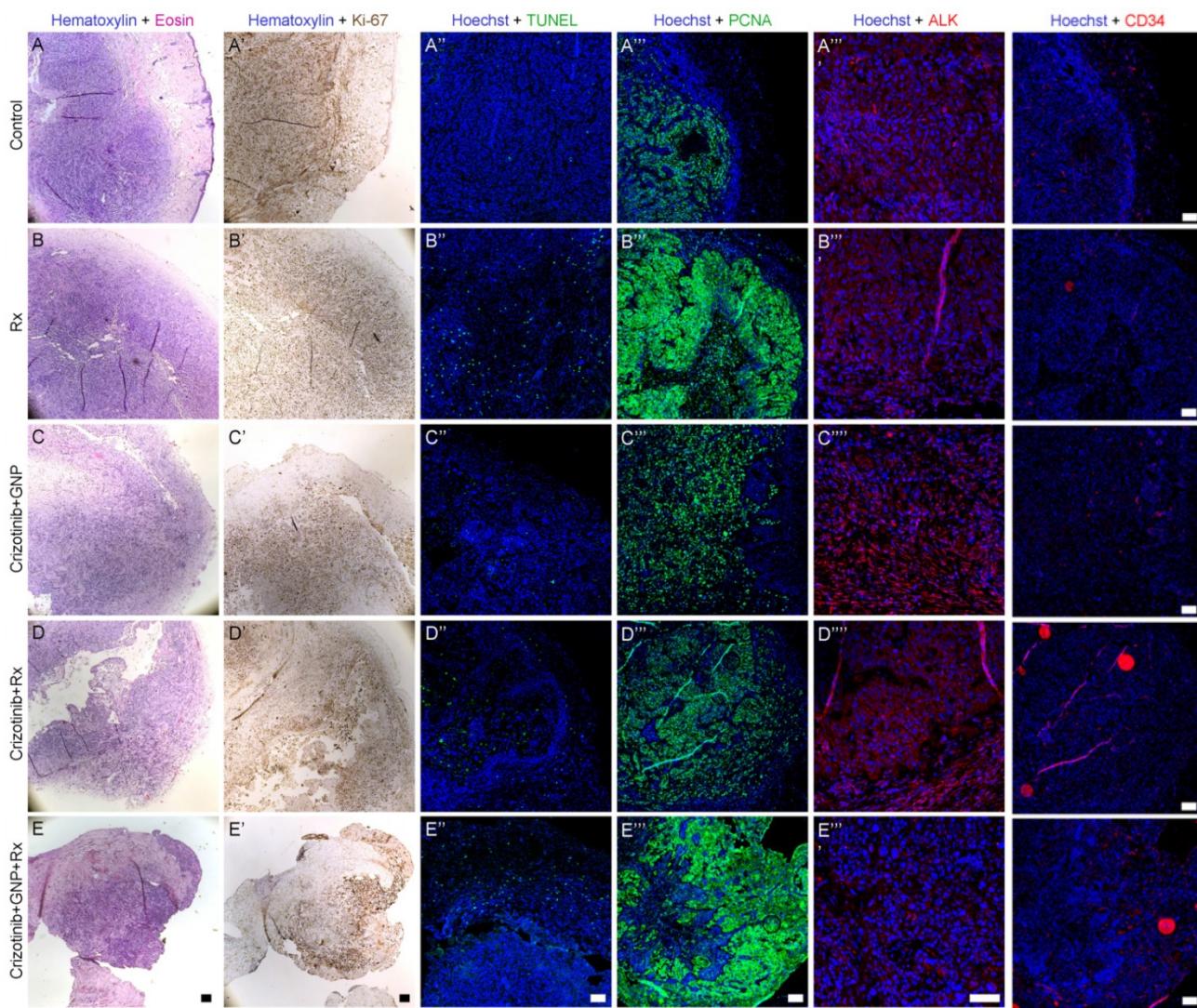

Figure 6: Histological characterization 24 days post treatments. Representative images of tumor sections and adjacent tissue are presented. Shown are saline administration (no treatment, A-A''''), radiation only (B-B''''), crizotinib-GNP (C-C''''), crizotinib-radiation (D-D'''') and radiation-crizotinib-GNP (E-E''''). Sections were stained with H&E (A-E), Ki-67 (A'-E', brown); TUNEL (A''-E'', green), PCNA (A'''-E''', green) ALK (A''''-E'''', red) and CD34 (red). Rx= radiation. Bar = 100 µm. Immunostaining intensity was analyzed using LSM software.

Treatment with crizotinib alone, or concomitantly with radiation, did not achieve major reduction in tumor size, though ALK was identified as a dominant mutation in the tumor. Thus, we assume that crizotinib serves as a vector and not as a treatment for ACC per se.

Enhancement of imaging using targeted GNP

A second goal in this study was to suggest a new concept in functional imaging, namely, targeted functional imaging. MRI, CT and PET/CT are complementary methods for detecting metastasis and perineural spread of ACC. However, PET/CT does not always detect perineural spread and micro metastases, because of variable FDG uptake and size limitations of this method. Furthermore, non-neoplastic conditions may cause false positive results[4,34].

Targeted functional imaging uses specific molecular probes instead of non-specific contrast materials, and thus offers early detection of cancerous cells that express specific surface receptors. This method can also characterize pathologies without invasive biopsies[34–37]. Hainfeld et al. showed that actively targeted GNP can enhance imaging of millimeter-sized human breast tumors in mice[38]. Others[20,39] have shown that small head and neck tumors, which are undetectable via CT, are enhanced and become visible by molecular targeted GNP.

Our study demonstrates that targeted GNP had a significant impact on tumor visualization and enhancement. The GNP concentrated in the tumor enabled simple and straightforward detection of ACC, while it was extremely difficult to identify in controls without GNP. Targeted GNP were not detected beyond the boundaries of the tumor, demonstrating the high accuracy of this method. These findings indicate that molecular profiling can greatly improve functional imaging.

Biological mechanism of targeted radiosensitizing GNP

As expected, ALK staining was similar in the untreated control and radiation-treated groups, confirming the presence of the ALK mutation in the tumor. Radiation did not cause degradation of ALK receptors. However, the addition of crizotinib to GNP or radiation resulted in stronger ALK staining. A possible explanation for this observation is that crizotinib induced stabilization and accumulation of ALK by inhibition of ALK phosphorylation and prevention of receptor ubiquitination, as described by Scaltriti et al. for a HER2 tyrosine kinase inhibitor[40]. The crizotinib-GNP-radiation treated mice showed the weakest ALK staining, indicating extensive damage to tumor DNA. The weak staining may also indicate that in this microscopic residual tumor, the only cells that were not affected by the treatment were those that did not present an ALK receptor. The strong PCNA and weak ki-67 staining observed herein suggest that damage to DNA, most probably secondary to apoptosis, is the main mechanism that enhances tumor radiosensitivity.

CD34 staining did not demonstrate a difference between the groups treated with or without GNP, therefore we assume that inhibition of angiogenesis is not a key mechanism for tumor destruction in ACC.

Toxicity

In the present study, only one mouse treated with crizotinib-GNP-radiation died before the end of the study, and no clinical evidence of toxicity was seen in the mice. We recently found that targeted GNP, via cetuximab, had no effect on well-being, hematology, and kidney and liver functions in mice[18], further supporting the safety of GNP for treatment. Additional studies are needed to fully evaluate the effect of crizotinib-GNP.

Despite the encouraging results of our study, some limitations need be considered when interpreting the results. The main limitation is the small number of mice in each group, due to the small amount of human tumor, lack of stable cell lines for ACC, and the low rate of tumor growth. In addition, the uniqueness of each tumor, as defined by the multiple different mutations that exist in each tumor, prevents repetition of the experiment.

In conclusion, this is the first study to demonstrate the potential use of molecular profile–guided targeted GNP for radiosensitization and functional imaging of tumors. Our findings suggest that intravenous administration of GNP that are selectively targeted to ACC can significantly increase the radiation absorbed in the tumor, as well as enable early diagnosis of ACC recurrence, and treatment follow-up. Thus, the current research indicates a promising role for molecular profiling as a tool to enhance both the imaging and radiosensitivity of tumors.

Materials & Methods

Patient accrual

The patient was accrued under an approved IRB protocol, and with informed consent in the Rabin medical center in Petach Tiqva.

Molecular profiling

For molecular profiling, a sample was taken from the patients' salivary gland ACC, and target genomic next generation sequencing was performed

via standard protocol. Briefly, 5μmeter sections of the formalin fixed paraffin embedded tumor resection block were marked for the cancer cell regions (identified from a consecutive cut stained with hematoxylin and eosin). DNA was extracted from the needle scratch of that region, using the standard protocol for Promega® robot. DNA was fragmented with COVARIS® and construction of next generation sequencing library (attachment of sample-specific index and the Illumina adaptors to DNA fragments) was performed with NEBnext™ kit. Target capture of an interval that includes all exons of 167 genes involved in a variety of carcinomas was performed using Agilent SureSelect. NGS was performed on Illumina® HiSeq2500™, eight samples on each lane (typically 25-30 million reads per sample). Reads were aligned to the reference genome, and subject to variant calling according to standard procedure (Lunke et al). The resulting VCF file was clinically annotated by comparing to reported recurrent and pathogenic variants using https://tgex-app. genecards.org/ (which sources data from http://www.sanger.ac.uk/genetics/CGP/cosmic/, http://pct.mdanderson.org and http://www. ncbi.nlm.nih.gov/clinvar and other repositories).

Transplantation of patient-derived xenografts

All animal experiments were carried out in compliance with the Israel Council on Animal Care regulations and were approved by the Institutional Animal Care University Committee of the Bar-Ilan University and Rabin Medical Center. 50 µl Human ACC was injected subcutaneously into the back flank area of 16 nude mice aged 10-11 weeks. Tumor volumes were measured twice weekly by electronic caliper for up to 24 days after treatment and by computed tomography (CT) at the end of treatment. When the tumor reached a diameter of 8-10 mm, the mice were divided into 6 groups and randomly allocated for treatment with radiation, crizotinib or GNP, alone and in various combinations; one group was untreated and served as a control.

Synthesis and characterization of GNP

The initial size and shape of the GNP were chosen according to previous study in which coated GNPs were used as contrast agents to improve CT imaging in head and neck cancer[20]. GNP were prepared as described by Enüstün and Turkevich[41]. In short, 414 µL of 50% w/v HAuCl4 solution were added to 200 mL purified water, the solution was heated in an oil bath until boiling. Then, 4.04 mL of sodium citrate tribasic dihydrate (Sigma-Aldrich) 10% solution was added and the solution was stirred for 10 min. After cooling to room temperature, the solution

was centrifuged again for additional hour. A protective layer of polyethylene-glycol (PEG) was then incorporated onto the surface to reduce nonspecific interactions and prolong the circulation time of the particles in the bloodstream[42]. The PEG layer consisted of thiol-polyethylene-glycol (HS-PEG-COOH) (MN ~1 kDa) (Sigma Aldrich). 120 µL of 50 mg/mL PEG solution was added to the GNP solution and stirred for 4 h at room temperature. Following this step, for active cancer cell targeting, the hetero-functional PEG was covalently conjugated to a crizotinib monoclonal antibody (Xalkori®, Sigma Aldrich). 200 µL of 10 mg/mL EDC solution (1-Ethyl-3-(3-dimethylaminopropyl) carbodiimide HCl) (Thermo Scientific) and 200 µL of 10 mg/mL NHS solution (N-Hydroxysulfosuccinimide sodium salt) (Sigma-Aldrich) were added to the nanoparticles solution. 5 minutes later, 200 µL crizotinib was added and stirred for additional 4 h at room temperature. Finally, centrifugation was performed until a final Au concentration of 30 mg/mL was achieved.

GNP characterization

Final particle size, shape, and uniformity were confirmed with transmission electron microscopy (TEM; JEM-1400, JEOL, Peabody, MA, USA). Samples were prepared by drop-casting 5 µL of the GNP solution onto standard carbon-coated film on a Copper grid and then left to dry in a vacuum machine. The GNP were further characterized at each stage using ultraviolet-visible spectroscopy (UV-1650 PC; Shimadzu, Kyoto, Japan) and measurement of the zeta potential (ZetaSizer 3000HS, Malvern Instruments, Worcestershire, UK). Crizotinib coating (200 µL; 25 mg/mL Au) were performed 12 hours before the experiment, and the GNP were administered to the test animals by injection into the tail vein. Table 2 summaries GNP characterization.

The amount of conjugated crizotinib was determined by the Bradford protein assay. By reducing the concentration of the unconjugated proteins from the total concentration of the proteins we were able to determine the concentration of the conjugated proteins. We then could further calculate the coupling ratio between the antibody and the particle which was determined to be 4 per particle.

Table 2. Characterization of GNP

	DLS (nm)	Zeta measurements (mV)
GNP without coating	**20± 2**	-38.9±1.04
GNP coated with PEG	**29.8±** 0.5	-22.09±0.98
GNP with PEG-crizotinib	**27.3±** 0.6	-19.62±0.85

Radiation

The mice were anesthetized, and x-ray irradiation was performed using a Varian linear accelerator (True Beam); the 6 MV flattening filter-free mode was chosen so the treatment could be delivered as quickly as possible (1.4 Gy per minute). The dose was administered to the measured depth. A customized bolus of 1 cm was designed for each mouse to ensure skin coverage, calculated according to the depth of each tumor. The field size was determined according to the tumor size (from1.5 x 1.5 to 2.0 x 2.0). Radiation was administered as a single fraction of 18 Gy.

Crizotinib

Crizotinib, alone or with radiation, was administered once at a dose of 2 mg per kg[42].

Micro CT scans

In vivo scans of mice were performed with nominal resolution (pixel size) of 36 microns, employing an aluminum filter 0.2 mm thick and an applied X-ray tube voltage of 45 kV. Surface-rendered 3D models were constructed for 3D viewing of the analyzed mice. Volume rendered 3D images were generated using an RGBA transfer function in SkyScan CT-Volume ("CTVol") software (Skyscan 1176, Bruker micro-CT, Kontich, Belgium), (NRecon v.1.6.9, Bruker micro-CT).All scans were performed under general anesthesia on life mice.

Flame Atomic Absorption Spectroscopy (FAAS)

FAAS, SpectrAA140, Agilent technologies. Labeled tissue was melted with aqua regia acid, a mixture of nitric acid and hydrochloric acid in a volume ratio of 1:3. The samples were then filtered and diluted to a final volume of 5 mL. An Au lamp was used in order to determine the gold concentration in the samples. A calibration curve with known gold concentrations was prepared (commonly: 0.1, 1, 2, and 5 mg/mL). Gold concentration in each sample was determined according to its absorbance value with correlation to the calibration curve. Each sample was analyzed in triplicate, and averages and standard deviations were taken.

Immunohistochemistry and confocal microscopy

The histological effect of radiation and biological agents was assessed using biopsy samples containing tumor and adjacent tissue that were taken from treated mice 24 days post treatment and further processed for histological analysis. Sections of fixed, paraffinized tumors and adjacent tissue were processed and incubated with primary antibodies: Mouse anti-ALK antibody [5A4] (1:50 ab17127 ,Abcam, USA) rabbit anti-Ki-67 (1:300; E1871; Spring Bioscience, CA, USA), rabbit anti-proliferating cell nuclear antigen (PCNA; 1:30; sc-7907; Santa Cruz Biotechnology) or rat anti-CD34 (1:200; CL8927AP, Cedarlane, Ontario, Canada). HRP-conjugated donkey anti-rabbit secondary antibody was used for immunoperoxidase Ki-67 staining. For immunofluorescence staining we used the following secondary antibodies: Alexa-555 conjugated goat anti-rat (1:400; Cell signaling technology, MA, USA) for CD34 staining and Alexa-488 conjugated donkey anti-rabbit (1:200; ab150065; Abcam, Cambridge, MA, USA) for PCNA staining. DNA was stained by Hoechst 33280 (1 µg/ml; Sigma). Images were photographed by LSM-510 confocal laser-scanning microscope (CLSM; Carl Zeiss MicroImaging, Oberkochen, Germany). Staining with secondary antibodies only served as negative control for immunofluorescence staining and was used for the photomultiplier offset calibration. Proliferation was assessed by quantification of Ki-67 positive cells per transverse sections of the tumor. At least 20 transverse sections from each treatment group were examined for each stain. Immunostaining intensity was analyzed using LSM software.

Apoptosis evaluation

DNA fragmentation was examined *in situ* on paraffin-embedded tumor sections in mice by terminal transferase-mediated dUTP nick-end labeling (TUNEL; DeadEndfluorometric TUNEL system, Promega, Madison, WI, USA) according to manufacturer's instructions. Sections exposed for 10 minutes to DNase I (6 units/ml; Invitrogen, Carlsbad, CA, USA) served as positive controls. Apoptosis was assessed by TUNEL positive cells per transverse sections of tumors and adjacent tissue. At least 20 transverse sections from each treatment group were examined for each stain. Immunostaining intensity was analyzed using LSM software.

Statistics

Differences between two means were tested using an unpaired, two-sided t-test. Immunostaining intensity was analyzed with repeated measures ANOVA. $p < 0.05$ was considered to be statistically significant.

Author contributions

I.H. designed and performed the experimental work, analyzed the data and wrote the manuscript. M.M and O.B conducted in vivo experiments and created statistical graphs, D.B and L.L planned and

performed radiation treatment. A.M assisted in analyzing the data. T.H performed statistical analysis. I.B.A and M.L analyzed the histological samples. I.H performed molecular profiling and identification of target mutation. T.S edited the manuscript. A.P and R.P proposed the hypothesis, designed the experimental procedures, approved the data analysis, wrote and edited the manuscript.

Competing Interests

The authors have declared that no competing interest exists.

References

1. Fordice J, Kershaw C, El-Naggar A GH. Adenoid Cystic Carcinoma of the Head and Neck. Arch Otolaryngol Head Neck Surg. 1999; 125:149–152.
2. Moskaluk C. Adenoid cystic carcinoma: clinical and molecular features. Head Neck Pathol. 2013; 7:17–22.
3. Shen C, Xu T, Huang C, et al. Treatment outcomes and prognostic features in adenoid cystic carcinoma originated from the head and neck. Oral Oncol. 2012; 48:445–449.
4. Coca-Pelaz A, Rodrigo J, Bradley P. Adenoid cystic carcinoma of the head and neck–an update. Oral Oncol. 2015; 51:652–661.
5. Roh J, Ryu C, Choi S, et al. Clinical utility of 18F-FDG PET for patients with salivary gland malignancies. J Nucl Med. 2007; 48:240–246.
6. National Comprehensive Cancer Network. NCCN clinical practice guidelines in oncology. head and neck cancers. 2016; .
7. Shultz D, Zeidan Y, Murphy J, et al. Radiotherapy for adenoid cystic carcinomas of the head and neck: clinical outcomes and patterns of failure. J Radiat Oncol. 2014; 3:49–56.
8. Mendenhall WM, Morris CG, Amdur RJ, et al. Radiotherapy alone or combined with surgery for adenoid cystic carcinoma of the head and neck. Head Neck. 2004; 26:154–162.
9. Iseli T, Karnell L, Graham S. Role of radiotherapy in adenoid cystic carcinoma of the head and neck. J Laryngol Otol. 2009; 123:1137–1144.
10. Hoff D Von, Stephenson J, Rosen P. Pilot study using molecular profiling of patients' tumors to find potential targets and select treatments for their refractory cancers. J Clin Oncol. 2010; 28:4877–4883.
11. Liu J, Shao C, Tan ML, et al. Molecular biology of adenoid cystic carcinoma. Head Neck. 2012; 34:1665–1677.
12. Bell D, Hanna E. Head and neck adenoid cystic carcinoma: what is new in biological markers and treatment?. Curr Opin Otolaryngol Head Neck Surgery. 2013; 21:124-129.
13. Lagha A, Chraiet N, Ayadi M. Systemic therapy in the management of metastatic or advanced salivary gland cancers. Head Neck Oncol. 2012; 4:1.
14. Stenman G, Persson F, Andersson M. Diagnostic and therapeutic implications of new molecular biomarkers in salivary gland cancers. Oral Oncol. 2014; 50:683–690.
15. Ross J, Wang K, Rand J, et al. Comprehensive genomic profiling of relapsed and metastatic adenoid cystic carcinomas by next-generation sequencing reveals potential new routes to targeted . Am J Surg Pathol. 2014; 38:235–238.
16. Popovtzer A, Sarfaty M, Limon D, et al. Metastatic Salivary Gland Tumors: A Single-Center Study Demonstrating the Feasibility and Potential Clinical Benefit of Molecular-Profiling-Guided Therapy. Biomed Res Int. 2015; 2015:1–7.
17. Dreifuss T, Betzer O, Shilo M, et al. A challenge for theranostics: is the optimal particle for therapy also optimal for diagnostics? Nanoscale. 2015; 7:2040–3364.
18. Popovtzer A, Mizrachi A, Motiei M, et al. Actively targeted gold nanoparticles as novel radiosensitizer agents: an in vivo head and neck cancer model. Nanoscale. 2016; 8:2678–2685.
19. Betzer O, Ankri R, Motiei M, et al. Theranostic approach for cancer treatment: Multifunctional gold nanorods for optical imaging and photothermal therapy. J Nanomater. 2015; 2015:646713.
20. Reuveni T, Motiei M, Romman Z, et al. Targeted gold nanoparticles enable molecular CT imaging of cancer: an in vivo study. Int J Nanomedicine 2011; 6: e64.
21. Li S, Huang L. Pharmacokinetics and biodistribution of nanoparticles. Mol Pharm. 2008; 5:496–504.
22. Rischin D, Peters LJ, O 'sullivan B, et al. Tirapazamine, Cisplatin, and Radiation Versus Cisplatin and Radiation for Advanced Squamous Cell Carcinoma of the Head and Neck (TROG 02.02, HeadSTART): A Phase III Trial of the Trans-Tasman Radiation Oncology Group. J Clin Oncol. 2010; 28:2989–2995.
23. Liu C, Wang C, Chen S, et al. Enhancement of cell radiation sensitivity by pegylated gold nanoparticles. Phys Med Biol. 2010; 55:931.
24. Chithrani D, Jelveh S, Jalali F, et al. Gold nanoparticles as radiation sensitizers in cancer therapy. Radiat Res. 2010; 173:719–728.
25. Hainfeld JF, Slatkin DN, Focella TM, et al. Gold nanoparticles: A new X-ray contrast agent. Br J Radiol. 2006; 79:248–253.
26. Hainfeld J, Slatkin D, Smilowitz H. The use of gold nanoparticles to enhance radiotherapy in mice. Cancer Res. 2005; 65:287–287.
27. Jong W De, Hagens W, Krystek P, et al. Particle size-dependent organ distribution of gold nanoparticles after intravenous administration. Biomaterials 2008; 1919–29:1912 ..
28. Iacono D, Chiari R, Metro G, et al. Future options for ALK-positive non-small cell lung cancer. Lung Cancer. 2015; 87:211–219.
29. Soda M, Choi YL, Enomoto M, et al. Identification of the transforming EML4–ALK fusion gene in non-small-cell lung cancer. Nature. 2007; 448:561–566.
30. Gridelli C, Peters S, Sgambato A, et al. ALK inhibitors in the treatment of advanced NSCLC. Cancer Treat Rev. 2014; 40:300–306.
31. Crescenzo R, Inghirami G. Anaplastic lymphoma kinase inhibitors. Curr Opin Pharmacol. 2015; 23:39–44.
32. Maeda H, Fang J, Inutsuka T, et al. Vascular permeability enhancement in solid tumor: various factors, mechanisms involved and its implications. Int Immunopharmacol. 2003; 3:319–328.
33. Kleibeuker EA, Griffioen AW, Verheul HM, et al. Combining angiogenesis inhibition and radiotherapy: A double-edged sword. Drug Resist Updat. 2012; 15:173–182.
34. Singh F, Mak S, Bonington S. Patterns of spread of head and neck adenoid cystic carcinoma. Clin Radiol. 2015; 70:644–653.
35. Kircher M, Hricak H, Larson S. Molecular imaging for personalized cancer care. Mol Oncol. 2012; 6:182–195.
36. Alberti C. From molecular imaging in preclinical/clinical oncology to theranostic applications in targeted tumor therapy. Eur Rev Med Pharmacol Sci. 2012; 16:1925–1933.
37. Pysz M, Gambhir S, Willmann J. Molecular imaging: current status and emerging strategies. Clin Radiol. 2010; 65:500–516.
38. Hainfeld JF, O'Connor MJ, Dilmanian FA, et al. Micro-CT enables microlocalisation and quantification of Her2-targeted gold nanoparticles within tumour regions. Br J Radiol. 2011; 84:526–533.
39. Popovtzer R, Agrawal A, Kotov N, et al. Targeted gold nanoparticles enable molecular CT imaging of cancer. Nano Lett. 2008; 8:4593–4596.
40. Scaltriti M, Verma C, Guzman M, et al. Lapatinib, a HER2 tyrosine kinase inhibitor, induces stabilization and accumulation of HER2 and potentiates trastuzumab-dependent cell cytotoxicity. Oncogene. 2009; 28:803–814.
41. Enustun B V., Turkevich J. Coagulation of Colloidal Gold. J Am Chem Soc. 1963; 85:3317–3328.
42. Zou H, Li Q, Engstrom L, et al. PF-06463922 is a potent and selective next-generation ROS1/ALK inhibitor capable of blocking crizotinib-resistant ROS1 mutations. Proc Natl Acad Sci U S A. 2015; 112:3493–3498.